Model for studies of laser-induced nonlinear processes in molecules

K. C. Kulander,[1] F. H. Mies,[2] and K. J. Schafer[3]
[1]*TAMP, Lawrence Livermore National Laboratory, Livermore, California 94551*
[2]*National Institute of Standards and Technology, Gaithersburg, Maryland 20899*
[3]*Department of Physics, Louisiana State University, Baton Rouge, Louisiana 70803*
(Received 3 November 1995)

The dynamics of strong-field ($\sim 10^{14}$ W/cm^2) multiphoton processes in molecules can be investigated using a simple, collinear model for H_2^+. We discuss properties of this model and report preliminary calculations related to recent experimental results. We find that the excitation and ionization dynamics of the molecular ion depend strongly on the laser wavelength, pulse shape, intensity, and particularly on the initial vibrational state of the molecule.

PACS number(s): 33.80.Rv, 33.80.Gj, 42.50.Hz

I. INTRODUCTION

There has been extensive progress over the past decade, both experimental and theoretical, in understanding the response of atoms to strong, short pulsed laser fields [1]. The situation for molecules [2] is not as advanced because of the higher level of complexity in systems with degrees of freedom that respond on very different time scales. However, the high degree of correlation between the electron and nuclear motions results in these systems being particularly interesting targets to probe with short pulse, high-intensity laser fields.

In studies of multiphoton excitation of molecules, one major focus has been to try to understand the competition between ionization and dissociation, that is, the partitioning of the absorbed energy between electronic and nuclear degrees of freedom. Most theoretical studies to date have invoked the Born-Oppenheimer (BO) separation of the electronic and nuclear degrees of freedom in addressing the multiphoton processes that occur. Electrons respond essentially instantaneously on the time scale of either the nuclear motion or the optical period of the laser field. However, as laser pulses become shorter and more intense, we should expect this approximation to break down. In a strong field the electronic structure of the molecule becomes distorted, differing substantially from its field-free BO state. As a result, very strong mixing between usually separable degrees of freedom becomes possible. Ionization and dissociation become intimately mixed and it ceases to be appropriate to interpret molecular behavior in very intense fields in terms of motion on a single or a few electronic surfaces.

One way to demonstrate this mixing of dissociative and ionizing dynamics would be to carry out calculations with all nuclear and electronic coordinates treated on an equal footing and then compare the results to the equivalent BO representation. For optical frequencies this is a formidable task, even for as simple a system as the hydrogen molecular ion [3], the subject of our studies here, unless some simplifying approximations are made. To this end we make the following two simplifications. First, we assume that the molecular axis is aligned along the laser polarization direction. It has been established, experimentally and theoretically, that in strong, linearly polarized laser fields, molecules rapidly become aligned with the field [4]. A second approximation, widely used in atomic studies [5], is to constrain the motion of the electron to a single dimension along the polarization direction. Although there is some coupling between the electron's longitudinal and transverse degrees of freedom because of the symmetry of the nuclear attraction potentials, the excitation dynamics is dominated by motion along the polarization axis in a strong laser field. Making these two assumptions allows us to reduce the spatial representation of this molecular system to two dimensions, the internuclear separation and the distance from the electron to the center of mass of the nuclei. This collinear model has the advantage that it can be solved either ''exactly'' numerically or by employing any of the usual simplifying assumptions. Also, because the wave function is two dimensional, we can display plots of the evolving probability density to interpret the excitation dynamics without excluding, freezing, or averaging over any additional dimensions. This is very helpful in discussing the competition between dissociation and ionization and in understanding the dynamics of Coulomb explosions [6,7] from field-distorted molecular configurations.

We will first present and discuss our collinear H_2^+ model, comparing its electronic structure and properties with those of the three-dimensional (3D) molecular ion. We show that this model has the physical characteristics that allow realistic investigations of the behavior of a molecule in a laser field. Next we discuss calculations for excitation by a strong, short pulse optical laser, investigating the properties of the evolving system both by analyzing the dynamics in terms of the BO states and by looking at snapshots of the time-dependent wave function. In particular, we show the dramatic difference a change in the initial vibrational level of the system makes in the excitation dynamics. Finally, we present ionization and dissociation results from this model, discussing them in the context of recent experimental studies [6,7] of molecular multiphoton processes.

II. MODEL FOR H_2^+

It is often very useful to explore the behavior of simplified models in order to understand complicated systems. One frequently employed simplification is to limit the number of dimensions in the model system to include only the most

active or most important coordinates. Because a strong, linearly polarized laser field tends to transfer its energy to electrons along the polarization axis, many useful and informative numerical experiments for atomic systems have been carried out by confining the electron motion to a single spatial dimension. The first to use this approximation for a multielectron system were Pindzola, Griffin, and Bottcher [8] (PGB), who investigated the dynamics of a model for helium in which the electrons were constrained to move only along the polarization axis. This reduced the problem to a manageable two spatial dimensions so that numerically exact calculations could be carried out and compared to those obtained using Hartree and single-active-electron approximation [9]. Additionally, PGB were able to visualize the excitation and ionization dynamics because the 2D wave function evolution could be followed completely using contour or three-dimensional surface plots. In this work PGB demonstrated that the Hartree wave function fails to represent the time-dependent dynamics accurately because of the importance of the correlated motion of the two electrons. In the Hartree wave function each electron responds only to the mean field of the other's probability distribution, not to its instantaneous position. This effect is expected to be even more important in a molecular system, where the motion of the electrons is very sensitive to the configuration of the nuclei.

We have applied the reduced dimensionality idea to H_2^+, where only the two most important coordinates, R, the distance between the protons, and z, the distance from the center of mass of the nuclei to the electron, are considered. This leads to the Hamiltonian given (in atomic units by)

$$H_0(R,z) = -\frac{1}{2\mu}\frac{\partial^2}{\partial R^2} - \frac{1}{2}\frac{\partial^2}{\partial z^2} + \frac{1}{\sqrt{R^2+q_n}} - \frac{1}{\sqrt{(z-R/2)^2+q_e}} - \frac{1}{\sqrt{(z+R/2)^2+q_e}}, \tag{2.1}$$

where μ is the reduced mass of the two nuclei and $q_n(q_e)$ is a screening parameter that softens the singularity when the nuclei (electron and nucleus) coincide. The elimination of the 1D singularities in the electrostatic interactions has been found to be a simple way to obtain realistic numerical results for multiphoton processes [5]. These parameters can be chosen to give the correct binding energy for the lowest state of the system.

We solve the time-dependent Schrödinger equation

$$i\frac{\partial}{\partial t}\Psi(R,z,t) = [H_0(R,z) + V_I(z,t)]\Psi(R,z,t) \tag{2.2}$$

for this collinear model of H_2^+ in a linearly polarized field using the dipole interaction between the electron and a classical, oscillating electric field of frequency ω:

$$V_I(z,t) = z f(t) \mathscr{E}_0 \sin(\omega t), \tag{2.3}$$

where $f(t)$ is the envelope function that turns the field on and off and $\mathscr{E}_0$ is the maximum field amplitude. The proton-laser interaction is negligible for the intensities considered here. We solve this two-dimensional problem "exactly" on a two-dimensional finite-difference grid. The grid is defined by $0.8 \leqslant R \leqslant 18.25$ with $\Delta R = 0.05$ and $-79.9 \leqslant z \leqslant 79.9$ with $\Delta z = 0.2$. Mask functions extend over the last 100–150 grid points on the outer R and z boundaries to remove flux and avoid reflections from these boundaries [10] and the time step used in integrating Eq. (2.2) corresponds to 1000–2000 steps per optical cycle. The screening parameters are chosen to be $q_n = 0.03$ and $q_e = 1.0$.

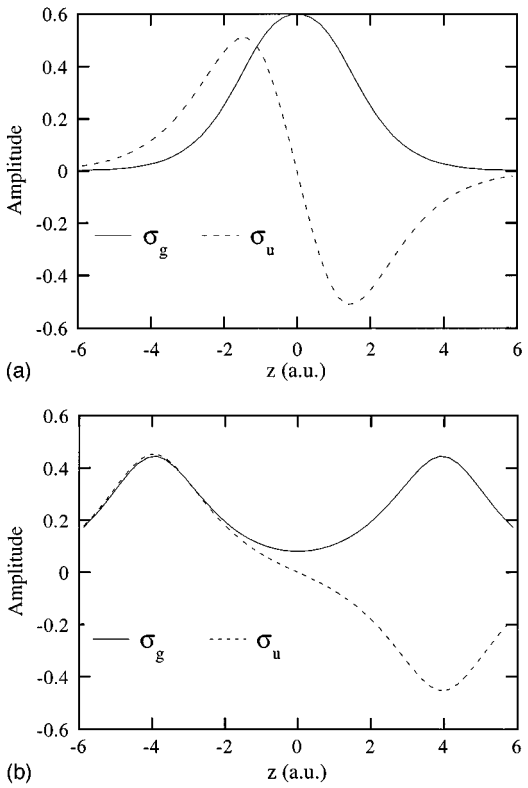

FIG. 1. Born-Oppenheimer, adiabatic wave functions for internuclear separations R of (a) $2.0a_0$ and (b) $8.0a_0$. In each plot the ground-state (gerade) and first excited-state (ungerade) orbitals are shown.

We find it helpful in interpreting our results to also consider the Born-Oppenheimer states that are obtained by fixing R and calculating electronic eigenfunctions. As an example, we show in Fig. 1 the wave functions for the two lowest BO states σ_g and σ_u for $R = 2.0a_0$ and $8.0a_0$ for the Hamiltonian in Eq. (2.1). In Fig. 1(b), the internuclear separation is large enough that the eigenvalues and, except for a change of sign at the midpoint between the nuclei, the amplitudes of the two wave functions on the two centers are becoming equivalent. As the nuclei separate, the atomic fragments, that is, the states with the electron associated with only one nucleus or the other, will be linear superpositions of these two molecular states. In Fig. 2 we compare the corresponding lowest two BO potentials of our model to those of the real system. The asymptotic energies of the ion-atom dissociation products for the two systems have been chosen to be the zero of energies for each pair of curves. As expected, the model σ_g ground state is bound and the σ_u excited state is repulsive. The asymptotic ionization potential of the real system is 13.6 eV, while for the 1D-model system it is 18.24 eV for $q_e = 1.0$ [11]. But, more importantly, the energy of first excited state in each case is about 10 eV. The

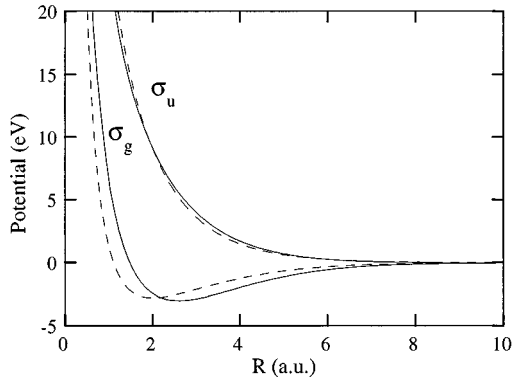

FIG. 2. Born-Oppenheimer potentials for collinear H_2^+. Solid lines are the model's potentials and the dashed lines are for the real 3D system.

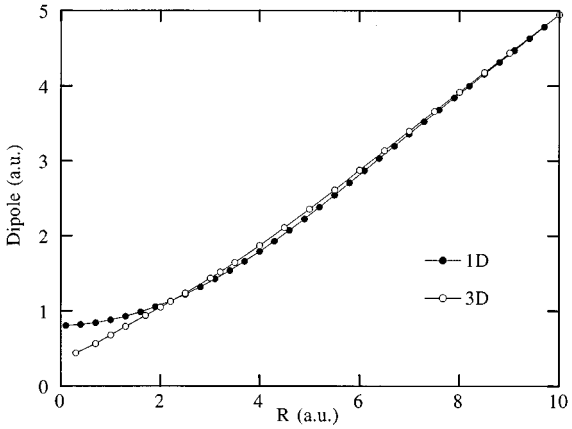

FIG. 3. Model and exact dipole transition strengths between the σ_g and σ_u BO molecular states.

main difference between the model and the real system is that the equilibrium separation is larger ($2.6a_0$ vs $2.0a_0$, respectively). For this choice of parameters the dissociation energy of the ground state turns out to be reasonably accurate (3.0 vs 2.8 eV). The ionization potential at the equilibrium geometry is 31.4 eV for the model and 29.9 eV for the real system. If we calculate the vibrational energy levels for this BO potential we find 21 levels, two more than in the real atomic ion. The harmonic (anharmonic) constant of 0.27 (5.5×10^{-3}) compares well with the 0.29 (7.6×10^{-3}) eV in the real molecule [12]. We note that it may be possible to make the electron-nuclear screening parameter, q_e, R dependent to improve the agreement between the model and real energies (i.e., in the united atom limit, we would need $q_e=0.5$ to obtain the correct ionization potential for He^+), but we have not tried to do that here.

We have also determined the R dependence of the transition dipole between the σ_g and σ_u states, given by

$$d(R)=\int \phi_g(z;R)z\phi_u(z;R)dz, \tag{2.4}$$

where $\phi_{g,\mu}$ are the BO states at internuclear separation R. These transition matrix elements, which strongly influence the multiphoton processes investigated here, are compared to the values for the 3D system [13] in Fig. 3. The agreement is very good over the range important for these studies, becoming poor only as the united atom limit is approached due to the fixed softening parameters used in the potentials. At large separation, it agrees well with the known $R/2$ asymptotic behavior.

Approximate BO *molecular* states are constructed as a direct product of the 1D (fixed-R) electronic states and the vibrational eigenfunctions calculated using the adiabatic BO potential. The *exact* ground and excited states are obtained by propagating the field-free time-dependent Schrödinger equation in imaginary time with the full two-dimensional potential [10]. We find the BO molecular states for the lowest several vibrational levels compare well with the exact states. Figure 4(a) shows the probability density for the state corresponding to the $v=4$ vibrational level. (Notice the appearance of the electronic density splitting in the outermost lobe.)

In the presence of a laser field, dissociation will occur when the wave-function amplitude travels to the right-hand edge of the grid [Fig. 4(a)], corresponding to large R, with density distribution being concentrated around $z\simeq\pm R/2$. On the other hand, photoionization of the molecular ion produces flux that moves either to the upper or lower boundaries of this grid (large $|z|$). We calculate the flux that crosses these respective boundaries by multiplying the wave function by masking functions after each integration step. The mask

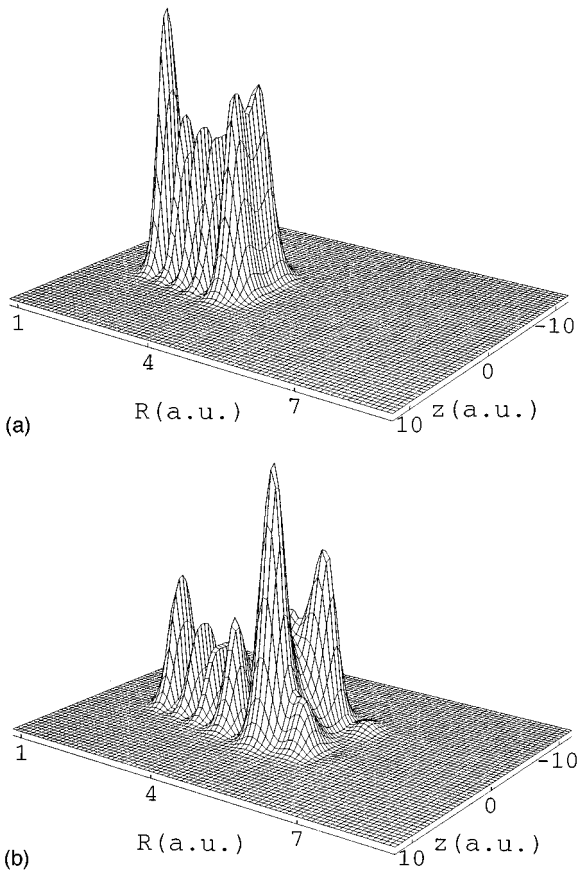

FIG. 4. (a) H_2^+ eigenfunction density distribution corresponding to the $v=4$ vibrational level of the nuclei. (b) Same state as above after the 770-nm laser field has been ramped over 12.5 optical cycles to an intensity of 1×10^{14} W/cm^2 and then held constant for an additional 2.5 cycles.

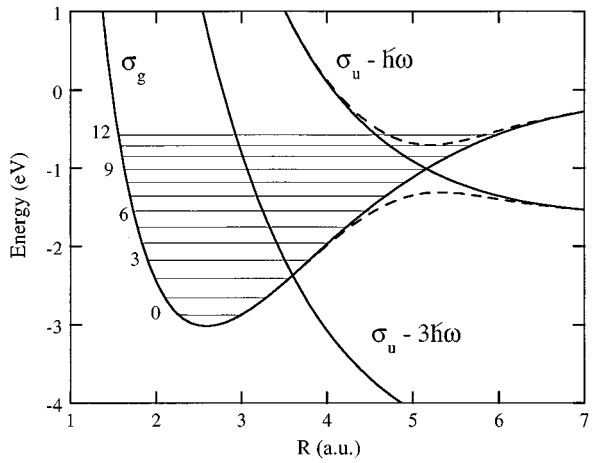

FIG. 5. Dressed molecular potentials showing crossings of the diabatic molecular states (solid curves) corresponding to the absorption of either one or three 1.61-eV ($\lambda = 770$ nm) photons. The lowest 13 field-free vibrational energies are shown within the σ_g well. The dashed lines show the adiabatic potentials for a laser intensity of approximately 6×10^{13} W/cm^2.

functions are unity over most of the grid, but gradually approach zero as either R or $|z|$ becomes large [10]. Decay rates, either for dissociation or ionization, can be determined from the reduction of the norm of the wave function remaining in the integation volume after the action of the appropriate mask.

In weak fields the excitation dynamics of this molecule can be well described in terms of the two lowest BO states. If we dress these BO states with photons by shifting the bare state potential curves by an integer number of photon energies, we find avoided crossings between the σ_g and σ_u states corresponding to one-photon and three-photon transitions [14]. The strengths of the avoided crossings depend on the amplitude of the laser's electric field. In Fig. 5 we show the diabatic, dressed states for a photon energy of 1.61 eV (770 nm). We also show the ''adiabatic'' states (dashed curves) created by the one-photon crossing near $5a_0$ for a laser intensity of 6×10^{13} W/cm^2. As the intensity increases the equilibrium separation of the lowest *adiabatic* state will become larger and the dissociation energy lower. The lower adiabatic well supports fewer bound vibrational states because of the possible transitions to the ungerade state at this crossing. This has been named ''bond softening'' [4]. This distortion of the potentials will be enhanced by higher-order crossings as the intensity is increased further. Vibrational levels in the excited (upper) adiabatic well will be quasibound (trapped), decaying only through the nonadiabatic coupling to the lower state. In Fig. 4(b) we show a snapshot of the ''dressed'' $v=4$ state created in a pulse that ramps to a peak intensity of 1×10^{14} W/cm^2 over 12.5 optical cycles and then is constant for 2.5 additional cycles. The charge density has shifted substantially to the region of the avoided crossing, apparently being partially captured in the upper adiabatic potential well. Such laser-induced states previously were predicted to exist in the real molecular ion [15] based on the BO dressed-state picture. They have been shown to contribute to population trapping [16,17] in short-pulse, strong-field dissociation of H_2^+. Recent measurements of electron [18] and proton [19] energy distributions from short-pulse high-intensity dissociation and/or ionization experiments have confirmed the existence of these trapped states. In the following sections we will discuss the role of this BO picture in the strong-field regime.

III. RESULTS

We consider the excitation, dissociation, and ionization dynamics for the ground ($v=0$) and the $v=4$ initial states. The chosen wavelength, 770 nm, has been used in several experimental and theoretical investigations and in recent two-state (BO) studies [17]. We use laser pulses that rise to peak intensities near 10^{14} W/cm^2 after a 12.5-cycle $\sin^2$ ramp. This intensity range is that which the molecular ion commonly experiences in subpicosecond laser experiments. The pulse ramp needs to be longer than those typically used in the time-dependent studies of atomic systems [20] because the molecular system has many low-lying vibrational levels. The excitation energies are a fraction of an electron volt (much less than the energy of a single photon) rather than the $\sim$10 eV typically encountered in rare-gas atoms. These levels are strongly mixed by a less adiabatic turn-on. Although the molecular state can be significantly distorted by the field [see Fig. 4(b)], this ramp is slow enough that there is little excitation of the neighboring levels for the $v=0$ case. After the ramp, the intensity is held constant for the rest of the calculation. In subsequent studies we will turn the field off again to determine the final-state populations.

We begin by examining results for the initial state $v=0$. In Figs. 6(a) and 6(b) we show the field-free and field-dressed states of the molecular ion for the peak intensity of 2×10^{14} W/cm^2. Before we discuss this case in detail we observe that the transition dipole, shown in Fig. 3, is large enough that at the peak of the field the Rabi frequency at the crossing point between the two dressed curves, given by $\mathscr{E}_0\cdot\mathbf{d}\approx\mathscr{E}_0(R/2)$, is 0.133 a.u. at 10^{14} W/cm^2. This is more than twice the laser frequency. Therefore we must consider the molecular system to be rapidly exchanging energy with the field, both absorbing and emitting photons, producing the field-dressed adiabatic potentials, which define the nuclear motion. This pulse is not strong enough to induce the trapping of the lowest few vibrational levels as discussed above, but it does produce a distortion of the effective internuclear binding potential, increasing the average distance between the nuclei. As the laser reaches its maximum intensity, we find the bond ''softens'' to a length 10–20 % larger than in the field-free state. By comparing Figs. 6(a) and 6(b) we see that for the $v=0$ case the peak in the charge distribution shifts from $R=2.6a_0$ to $3.1a_0$.

In order to follow the disposition of the absorbed energy within the molecule during this pulse it is useful to calculate several properties of the time-dependent wave function. In Fig. 7 we show the evolution of the total norm of the wave function remaining on the grid and the cumulative ionization and dissociation probabilities. The primary decay mechanism in this case is ionization. In all studies we present here, the intensity was high enough that both dissociation and ionization were observed, with ionization becoming dominant at higher intensities. The time-dependent expectation value of R,

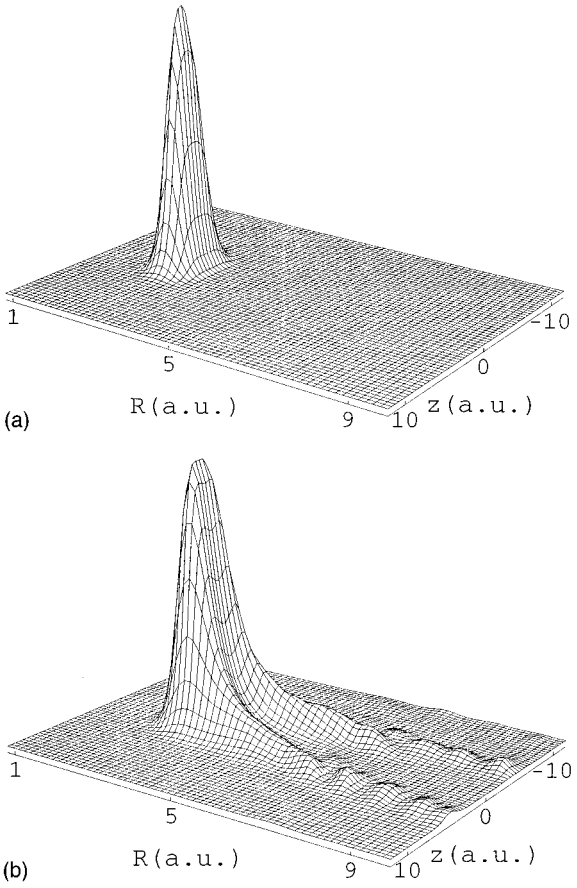

FIG. 6. H_2^+ density distributions for (a) the ground state ($v=0$) and (b) after 50 cycles of a pulse with a peak intensity of 2×10^{14} W/cm^2 at 770 cm.

$$\langle R(t)\rangle = \int\int |\Psi(R,z;t)|^2 R\, dR\, dz \Big/ \int\int |\Psi(R,z;t)|^2 dR\, dz, \tag{3.1}$$

also shown in Fig. 7, increases by an amount even greater than the shift in the peak noted above due to the probability density moving toward the large-R boundary. Because we remove this dissociating flux at a finite value of R, this expectation value remains finite. In this case $\langle R(t)\rangle$ is found to reach a steady state as the rate of decay (dissociation plus ionization), calculated from the decrease in the wave function norm, becomes constant. From these results we learn that this initial state is distorted by the field, then decays at the peak intensity predominantly by ionization at a rate which becomes constant with time. Thus the system seems to evolve to a sort of quasienergy state one might obtain from a Floquet calculation at this constant intensity.

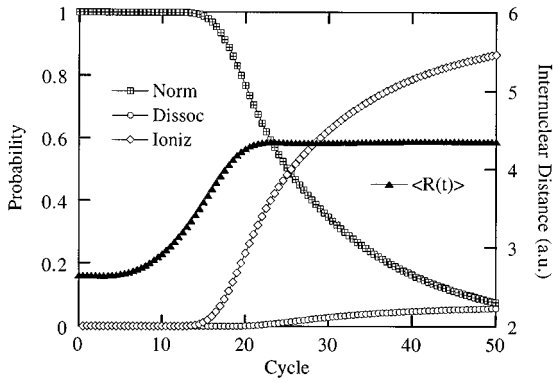

FIG. 7. Time-dependent expectation values for initial state $v=0$ in a ramped 770-nm laser field with a peak intensity of 2×10^{14} W/cm^2.

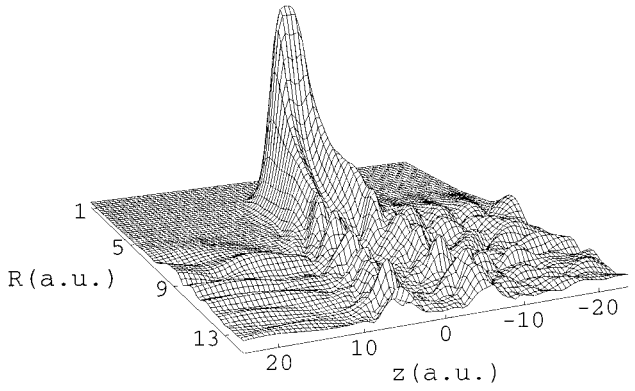

FIG. 8. H_2^+ wave-function *amplitude* after 50 cycles of a 770-nm ramped laser field with a peak intensity of 2×10^{14} W/cm^2. The initial state was the $v=0$ state.

In Fig. 8 we show a snapshot of the wave function *amplitude* (the square root of the density) after the 50th cycle. [The same wave function whose density is shown in Fig. 6(b).] Plotting the amplitude emphasizes the weaker, ionizing components of the wave function. At large R the electron density that remains bound (corresponding to $H^+ + H$) separates to follow one nucleus or the other. The ionization flux, evident on both sides of the molecule, moves toward the ionization boundaries for all R greater than $\sim 5a_0$. Although we find that ionization dominates over dissociation, the probability density correpsonding to the latter channel appears more pronounced in the plots because of the lower velocity of the protons.

In addition, we find a surprising effect in this case. At a particular R, the dissociating charge density appears to be concentrated around either one proton or the other. An alternation in the density distribution (with R) is clearly evident. This may be seen more easily in Fig. 6(b). By watching the time evolution of the wave function, we see that this is induced by the oscillation in the instantaneous direction of the electric field. Dissociation is initiated as the field reaches its maximum, at which time the electron is pushed toward one end of the molecule or the other, depending on the sign of the field. One-half cycle later another burst of dissociation occurs, but now with the electron driven toward the opposite end of the molecule. This effect was found to be most pronounced for this particular wavelength, peak intensity, and initial vibrational state. For other conditions the alternation was less dramatic or entirely absent, indicating the importance of the detailed structure of the field-dressed potentials and initial state.

In Fig. 9 we have plotted the time-dependent radial density distribution obtained from the wave function by integrat-

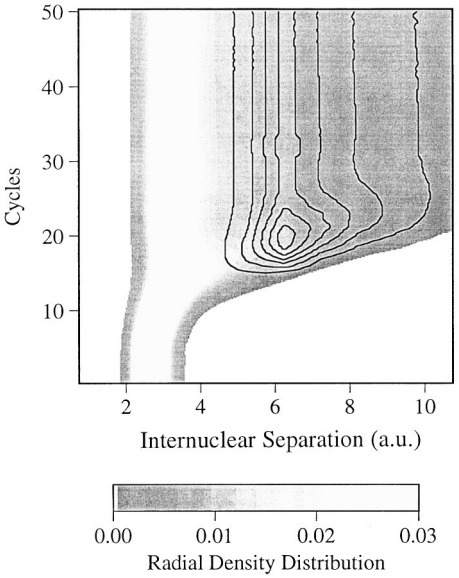

FIG. 9. Shaded plot shows the radial probability distribution as a function of time for the 50-cycle pulse shown in Figs. 6–8. Contours indicate the calculated R-dependent ionization rates.

ing over the electronic coordinate

$$P(R;t)=\int |\Psi(R,z;t)|^2 dz. \tag{3.2}$$

Initially we see the peaked distribution of the ground state, which, as the intensity reaches its maximum after 12.5 cycles, is distorted and begins dissociating. The peak of the bound component has shifted as described above by about 20 % and the dissociating flux propagates toward the large-R boundary. We can estimate the distribution of internuclear separations at which ionization occurs by binning the flux crossing the large-$|z|$ boundaries. Taking the time derivative of the probability flux reaching the z gobbler within $1a_0$-wide R bins, we can define time- and position-dependent rates of the ionization. Because of the size of the grid some propagation time elapses before the electron reaches the gobbler (i.e., it is removed by the z-boundary mask function). During this time the loss of screening between the nuclei causes these ''exploding'' components of the wave function to move toward larger R. Therefore the electron reaches the boundary at an internuclear separation that is slightly larger than where it was initially freed. By varying the distance to the gobbler we find that this shift is not very significant. If the nuclei are separating with an energy on the order of 1 eV, their relative velocity is approximately $1a_0$ per optical cycle. Electrons with drift energies near the ponderomotive energy ($e^2E^2/4m\omega^2$) in this field reach the boundary in much less than a cycle ($v>1$ a.u.).

The results of this flux analysis for this case are also shown in Fig. 9. Superimposed on the radial distributions are contours indicating the R-dependent ionization rate. Ionization is most rapid immediately following the not quite adiabatic turn-on. These partial rates, which have been scaled by the time-dependent norm, appear to become constant after the initial transient excitations have passed. The R-dependent rate exhibits a broad maximum around a finite

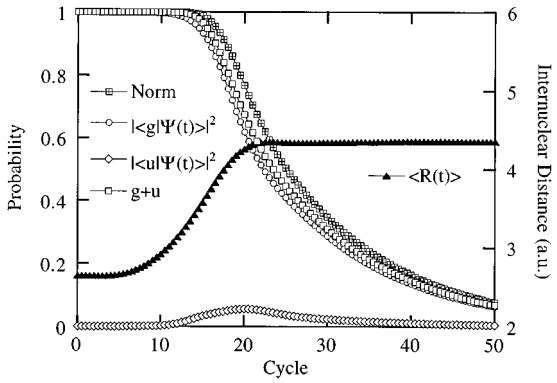

FIG. 10. BO projections of the total time-dependent wave function onto the R-dependent σ_g and σ_u for the case shown in Figs. 6–8.

value of the internuclear separation. The peak in the R-dependent rate is due to a combination of the ionization rate increasing and the probability density decreasing as the internuclear separation becomes larger. The ionization rate increases because the electronic binding energy is a decreasing function of R. As probability density moves toward larger R it is rapidly ionized. In this case, some small fraction survives to escape through our large-R boundary (dissociation). Because the ionization rate at this wavelength and intensity is large even for the isolated atom (1.5×10^{13} s^{-1}), the fragment atoms would be ionized before they leave the focal volume. By putting out detector (R gobbler) unphysically close to the molecule, we have overestimated the dissociation probability and therefore underestimated the ionization probability an equivalent amount. At lower intensities for which the ionization rate does not result in postdissociation ionization, the probabilities we calculate will be more accurate.

Much of the previous discussion has made use of the traditional view of molecular behavior, that is, in terms of internuclear potentials appropriate to the BO approximation. In H_2^+, the laser strongly couples the two lowest electronic states and most of the previous multiphoton studies have included only these states. Our complete calculation allows us to test the validity of this picture, since we can project our time-dependent wave function onto these BO states,

$$p(t)=\left|\int\int \phi_p(z;R)\Psi(R,z;t)dR\,dz\right|^2, \tag{3.3}$$

where $\phi_p(z;R)$ is the pth BO state at internuclear separation R. In Fig. 10 we show the time-dependent projections of the σ_g and σ_u states compared to the total norm. For this case there is a significant deficit between the sum of the projected probabilities and the norm, indicating the presence of excited electronic components. A similar calculation at 1053 nm shows no comparable probability in excited states, indicating that the effect shown in Fig. 10 is most likely due to the resonant excitation of a slowly ionizing state. Because the resonance energies are R dependent, the role of excited states varies not only with wavelengths and intensities, but depends on the radial distribution (vibrational state) also.

If the initial state is (vibrationally) excited, the response to the laser field can be quite different. To illustrate this we next

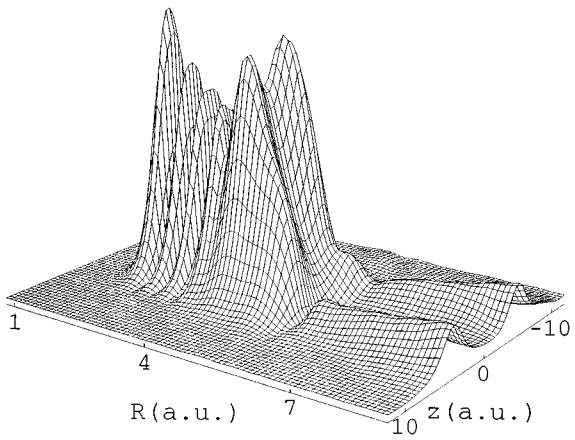

FIG. 11. H_2^+ wave-function amplitude after 100 cycles of a 770-nm ramped laser field with peak intensity of 8×10^{13} W/cm^2. The initial state was the $v=4$ state.

consider two cases starting in the $v=4$ state. In Fig. 11 a snapshot of the time-dependent wave function after 100 optical cycles of a 770-nm laser with a peak intensity of 8×10^{13} W/cm^2 is shown. By comparing to Fig. 4(a) we see the remnant of the initial ''diabatic'' state, along with a large amplitude centered near $5a_0$, where the avoided crossing occurs. This clearly shows the existence of an adiabatic laser-induced bound state. The small-R part of the wave function is actually quite different from the initial state both because the interaction with the ungerade state has modified the shape of the lower (mostly) gerade BO well and because other vibrational states have become populated.

As before, we evaluate the time-dependent wave function norm, the dissociation and ionization probabilities, and the expectation value of the internuclear separation. These are shown in Fig. 12, where we have followed the evolution over 100 optical cycles because of the rather slow decay of the transients during the ramp. We find that in this case the main decay channel is dissociation. In contrast to the previous case, $\langle R(t)\rangle$ exhibits strong oscillatory behavior during the constant intensity part of the pulse. There is also pronounced structure in the total and the dissociation decay probabilities that appears to be related to the oscillations in the radial distribution. However, because of the delay due to the finite

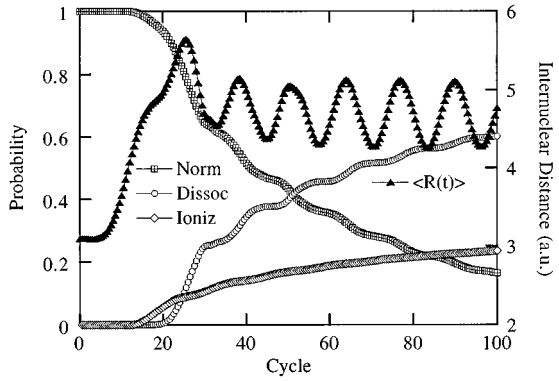

FIG. 12. Time-dependent expectation values for initial state $v=4$ in a ramped 770-nm laser field with a peak intensity of 8×10^{13} W/cm^2.

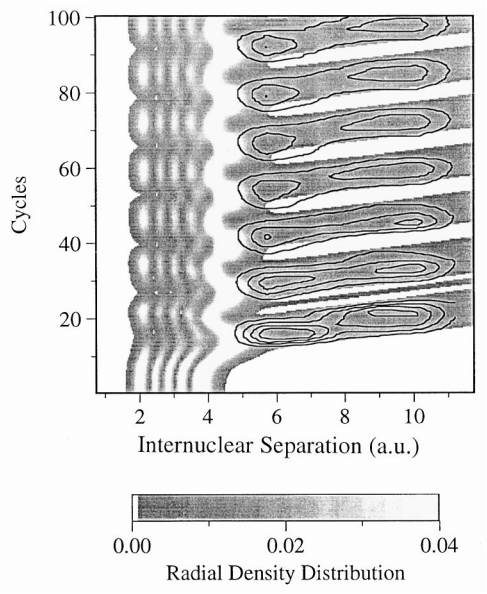

FIG. 13. Shaded plot shows the radial probability distribution as a function of time for the 100-cycle pulse shown in Figs. 11 and 12. Contours indicate the calculated R-dependent ionization rates for this $v=4$, 8×10^{13} W/cm^2 case.

propagation time to the dissociation boundary, this connection cannot be established from the results in this figure alone. Examination of the time-dependent radial probability distributions in Fig. 13 shows clearly that there is a resonance between the vibrational state located within the σ_g well and a trapped state centered near the avoided crossing [21]. Just after the ramp there is a substantial amount of probability beginning to dissociate as in the previous, $v=0$, case, but some fraction of it is caught within the upper adiabatic well. After several cycles, this trapped population leaks back onto the lower adiabatic potential mostly returning to a state that resembles the $v=4$ initial state. This process is repeated several times during the 100 cycles shown, with a period of approximately 12–13 cycles. During the trapping periods there is clearly a marked decline in dissociation. Then as the probability flows back into the diabatic state, some fraction leaks out and dissociates. An estimate of the velocity of the dissociating fragments can be obtained from the slope of the dissociating flux in this figure. It is approximately 1 eV, which is consistent with the molecule having

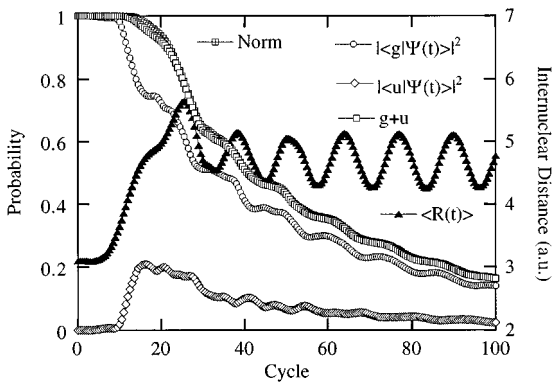

FIG. 14. BO projections of the total time-dependent wave function for the $v=4$, 8×10^{13} W/cm^2 case.

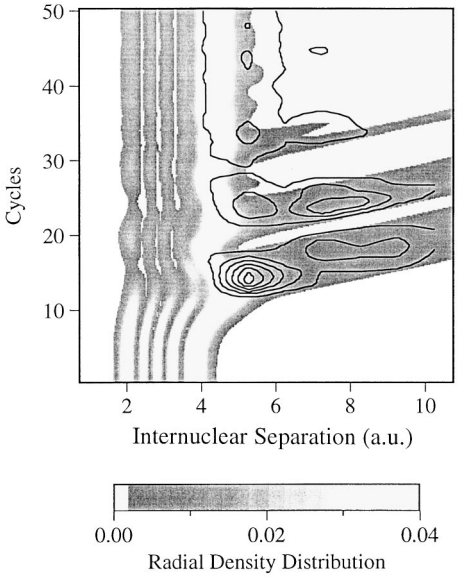

FIG. 15. Shaded plot shows the radial probability distribution as a function of time for the 50-cycle pulse for the $v=4$, 1×10^{14} W/cm^2 case. Contours indicate the calculated R-dependent ionization rates.

absorbed two photons. (See Fig. 5.) It is interesting to compare the final radial probability distribution at the end of the 100th cycle in Fig. 13 with the total wave-function density in Fig. 11. The minimum in the dissociative flux just beyond the trapped state is evident. Also the bimodal structure of the electronic state for large R shows the relative probability that the electron is on one fragment nucleus or the other does not vary with time. The asymmetry in dissociation observed in the $v=0$ case is absent here. Of course, in both cases the time-averaged probability is symmetric.

Figure 13 shows that the radial dependence of the ionization is again concentrated in the large-R region and correlates exactly with the dissociative flux. The time-dependent electronic state is well represented in terms of the two BO states, as shown in Fig. 14. There is no significant difference between the sum of the g and u components and the total norm on the grid.

The final case we will consider is the same as the previous one but with a higher intensity 1×10^{14} W/cm^2. In this case, the transient excitation produced during the ramp decays rather quickly and the system becomes stably trapped after about 30 cycles. This can be seen most clearly from the time dependence of the radial distribution shown in Fig. 15. In Fig. 16 the decay curves show that a large fraction of the initial wave function escapes immediately, and then the ionization and dissociation rates drop dramatically. Ionization exceeds dissociation at this intensity, whereas the reverse was true in the previous case. Again we find the ionization that occurs is predominantly at large R, with the rate peaking just beyond the separation where the radial distribution is concentrated. Very little dissociation occurs once this stabilized state has been established. The projections on the BO states are shown in Fig. 17. Most of the probability remains in the two lowest states and the gerade and ungerade components are comparable. We would expect an adiabatic trapped state would have equal amplitude in these two states,

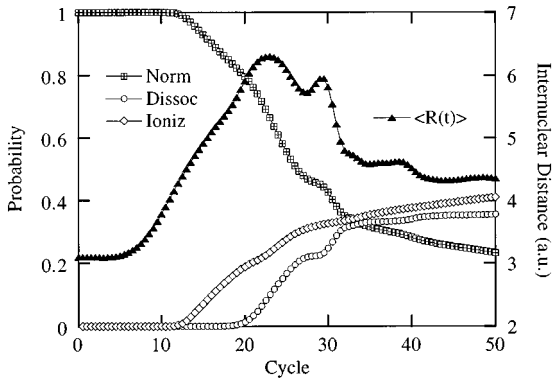

FIG. 16. Time-dependent expectation values for initial state $v=4$ in a ramped 770-nm laser field with a peak intensity of 1×10^{14} W/cm^2.

but since the plotted probabilities are averaged over all R, the σ_g projection is larger because of the short-range contribution to the integral being essentially pure gerade. While the system remains trapped, we see neither dissociation nor the flow back into the diabatic states.

IV. CONCLUSIONS

We have presented results for multiphoton dynamics of the hydrogen molecular ion using a simple, collinear model that does not require the usual separation of the electronic and nuclear degrees of freedom. We found that at approximately 10^{14} W/cm^2 and 770 nm both dissociation and ionization are important and that the excitation dynamics can be very different for different initial vibrational states. In the $v=0$ case we found that the system evolves to a distorted, constantly decaying state with a shifted equilibrium bond length.

Bond softening has been observed in several multiphoton dissociative ionization experiments, which uniformly show that the energy release is at most 70–80 % of that expected from the field-free equilibrium separation [6]. This should be expected to happen in any system that has a nearby repulsive electronic state that is strongly coupled to the ground state. In a laser pulse this distortion will occur before the intensity is high enough for ionization (Coulomb explosion) to become significant, so that the observed energy of the fragments will be less than that predicted based on the field-free

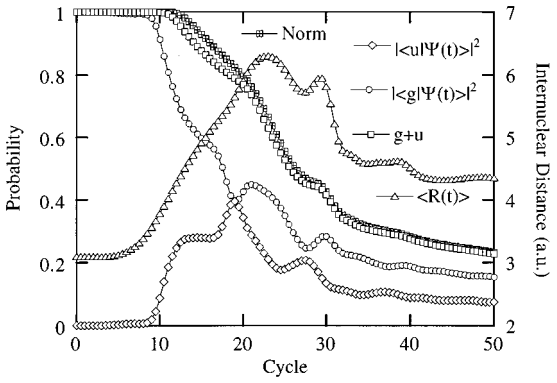

FIG. 17. BO projections of the total time-dependent wave function for the $v=4$, 1×10^{14} W/cm^2 case.

bond lengths. It has been pointed out recently that the observed Coulomb explosion fragment velocities are apparently also strongly affected by a very considerable enhancement of the tunneling ionization rate for bond lengths near and just beyond where the symmetric and antisymmetric wave functions become degenerate [22,23,3].

For the higher excited initial state, trapping and inhibition of dissociation were found. It appears that there is a range of vibrational levels that can become trapped. Even though the field free energy of the $v=4$ state is well below the upper adiabatic well (Fig. 5), the laser field was able to promote most of the density into the quasibound levels, shutting down dissociation. The lowest states were found to be merely distorted by these fields and the highest ones are easily dissociated. It was particularly useful in analyzing the excitation dynamics to have the abilities both to visually follow the evolution of this two-dimensional wave function and to project the time evolving states onto the field-free and dressed BO states. Although the major components of the wave function are the lowest two BO states, bound excited states can be important under specific conditions. We believe we have shown that the collinear system provides a useful representation of the real molecular ion. The results obtained are relevant to any diatomic in a strong linearly polarized field.

ACKNOWLEDGMENTS

This work was carried out in part under the auspices of the U.S. Department of Energy at the Lawrence Livermore National Laboratory under Contract No. W-7405-ENG-48. K.C.K. would like to acknowledge the kind hospitality of the Joint Institute for Laboratory Astrophysics at the University of Colorado, where some of this work was carried out.

[1] *Atoms in Intense Laser Fields*, edited by M. Gavrila (Academic, San Diego, 1992).

[2] *Molecules in Laser Fields*, edited by A. D. Bandrauk (Dekker, New York, 1994).

[3] Some high-frequency results have been obtained in three dimensions. See S. Chelkowski, T. Zuo, O. Atabek, and A. D. Bandrauk, Phys. Rev. A **52**, 2977 (1995), and references therein.

[4] P. H. Bucksbaum, A. Zavriyev, H. G. Muller, and D. W. Schumacher, Phys. Rev. Lett. **64**, 1883 (1990); A. Zavriyev, P. H. Bucksbaum, H. G. Muller, and D. W. Schumacher, Phys. Rev. A **42**, 5500 (1990); E. Charron, A. Giusti-Suzor, and F. H. Mies, *ibid.* **49**, R641 (1994).

[5] J. H. Eberly, R. Grobe, C. K. Law, and Q. Su, in *Atoms In Strong Fields*, edited by M. Gavrila (Academic, Boston, 1992), p. 301.

[6] K. Codling, L. J. Frasinski, and P. A. Hatherly, in *Multiphoton Processes*, edited by G. Mainfray and P. Agostini (CEA, Saclay, 1991); M. Schmidt, D. Normand, and C. Cornaggia, Phys. Rev. A **50**, 5037 (1994).

[7] W. T. Hill III, J. Zhu, D. L. Hatton, Y. Cui, J. Goldhar, and S. Yang, Phys. Rev. Lett. **69**, 2646 (1992); H. Stapelfeldt, E. Constant, and P. B. Corkum, *ibid.* **74**, 3780 (1995).

[8] M. S. Pindzola, D. C. Griffin, and C. Bottcher, Phys. Rev. Lett. **66**, 2305 (1991).

[9] K. C. Kulander, Phys. Rev. A **36**, 2726 (1987).

[10] K. C. Kulander, Phys. Rev. A **35**, R445 (1987); J. L. Krause, K. J. Schafer, and K. C. Kulander, *ibid.* **45**, 4998 (1992).

[11] Q. Su and J. H. Eberly, Phys. Rev. A **44**, 5997 (1991).

[12] K. P. Huber and G. Herzberg, *Molecular Structure and Molecular Spectra IV. Constants of Diatomic Molecules* (Van Nostrand Reinhold, New York, 1979).

[13] J. M. Peek and M. M. Madsen, Phys. Rev. A **43**, 147 (1991).

[14] A. I. Voronin and A. A. Samokhin, Zh. Éksp. Teor. Fiz. **70**, 9 (1976) [Sov. Phys. JETP **43**, 4 (1976)]; J. M. Yaun and T. F. George, J. Chem. Phys. **68**, 3040 (1978); A. D. Bandrauk and M. L. Sink, Chem. Phys. Lett. **57**, 569 (1978).

[15] A. D. Bandrauk and M. L. Sink, J. Chem. Phys. **74**, 1110 (1981); A. Giusti-Suzor, X. He, O. Atabek, and F. H. Mies, Phys. Rev. Lett. **64**, 515 (1990).

[16] A. Giusti-Suzor and F. H. Mies, Phys. Rev. Lett. **66**, 3869 (1992); G. H. Yao and S. I. Chu, Chem. Phys. Lett. **197**, 663 (1992); J. Y. Wang and S. I. Chu, *ibid.* **227**, 663 (1994); E. E. Aubanel, J. M. Gauthier, and A. D. Bandrauk, Phys. Rev. A **48**, 2145 (1993); E. E. Aubanel, A. Conjusteau, and A. D. Bandrauk, *ibid.* **48**, R4011 (1993).

[17] A. Giusti-Suzor, F. H. Mies, L. F. DiMauro, E. Charron, and B. Yang, Top. Rev. J. Phys. B **28**, 309 (1995).

[18] S. W. Allendorf and A. Szöke, Phys. Rev. A **44**, 518 (1991).

[19] A. Zavriyev, P. H. Bucksbaum, J. Squier, and F. Saline, Phys. Rev. Lett. **70**, 1077 (1993).

[20] K. C. Kulander, K. J. Schafer, and J. L. Krause, in *Atoms in Intense Laser Fields*, edited by M. Gavrila (Academic, San Diego, 1992), p. 247.

[21] A. D. Bandrauk, J. M. Gautier, and J. F. McCann, J. Chem. Phys. **100**, 340 (1994).

[22] J. H. Posthumus, L. J. Frasinski, A. J. Giles, and K. Codling, J. Phys. B **28**, L349 (1995); T. Seideman, M. Yu. Ivanov, and P. B. Corkum, Phys. Rev. A **75**, 2819 (1995).

[23] F. H. Mies, K. C. Kulander, and K. J. Schafer (unpublished).